Sensitivity Modeling of an RFID-Based Strain-Sensing Antenna with Dielectric Constant Change

Xiaohua Yi, Terence Wu, *Student Member, IEEE*, Yang Wang, *Member, IEEE*, Manos M. Tentzeris, *Fellow, IEEE*

Abstract— **An RFID (radiofrequency identification)-based folded patch antenna has been developed as a novel passive wireless sensor to measure surface strain and crack, for the structural health monitoring of metallic structures. Up to 2.5 meters of read range is achieved by a proof-of-concept prototype patch antenna sensor with a strain sensitivity around -760 Hz/με, which is equivalent to a normalized strain sensitivity of -0.74 ppm/με. In this paper, we propose to consider the change of the substrate dielectric constant due to strain when modeling the antenna sensor. An enhanced strain sensitivity model is introduced for more accurately estimating the strain sensing performance of the hereby introduced "smart skin" antenna sensor. Laboratory experiments are carried out to quantify the dielectric constant change under strain. The measurement results are incorporated into a mechanics-electromagnetics coupled simulation model. Accuracy of the multi-physics coupled simulation is improved by integrating dielectric constant change in the model.**

Index Terms— **Folded patch antenna, RFID sensor, structural health monitoring, smart skin, dielectric constant change, antenna sensor, wireless sensor, strain sensing.**

I. INTRODUCTION

STRUCTURAL health monitoring (SHM) systems utilize sensing technologies to monitor the condition of a structure (e.g. a mechanical, civil, or aerospace structure) in order to facilitate maintenance and retrofitting decisions [1]. Among the various engineering demands involved in SHM, the early detection of cracks in metallic structures (e.g. steel bridges or aluminum ships) has long been an important and challenging issue.

In an SHM system, stress/strain concentration is usually monitored as an indicator for fatigue or crack formation. Most of the current strain sensing techniques, such as metal foil strain gauges or fiber optic sensors, require cabled installation of the sensor and associated data acquisition system [2, 3]. To eliminate the high cabling cost for large structures, wireless sensing devices have been developed for digitizing and transmitting sensor data [4, 5]. These devices usually require batteries or energy harvesters for power supply. For example, a number of energy harvesting techniques have been proposed [6-8]. In particular, the WISP (Wireless Identification and Sensing Platform) system offers a wireless power harvesting platform for strain measurements [9]. A WISP node contains a built-in microcontroller, a voltage regulator, and power harvesting components, among others. The microcontroller performs analog-to-digital conversion to the analog signal from a typical metal foil strain gauge, and wirelessly transmits digitized data using a built-in modulator and demodulator.

Other researchers have proposed passive wireless strain sensing through analog mechanisms to reduce the complexity of the wireless nodes [10-14]. This passive approach removes the process of onboard digitization, eliminates the requirement for a microcontroller in the sensor node, and usually entails an electromagnetic antenna with known resonance frequency. Upon firmly attaching the antenna to a structure and allowing its shape to change with the strain in the structure, the resonance frequency of the antenna shifts accordingly with strain. This enables the wireless reading of analog information without the use of onboard ADC circuits and RF amplifiers, thus greatly simplifying the sensor design and reducing power requirement. In [10] and [11], the authors introduced wireless measurement with an inductive loop. However, inductive loops have limited communication range, which can be even more limited near metallic structural surfaces. The cylindrical cavity method proposed in [12] offers high Q response for detection, but can be costly to implement and difficult to attach to the surface of a flat metallic structure. Deshmukh and Huang [14] introduced a patch antenna that achieved 1 meter of read range on metallic objects with the use of a photodiode circuitry.

Through the utilization of RFID sensors [15], the passive antenna sensor studied in our research improves the wireless read range by a factor of at least 2-3, reduces fabrication cost,

Xiaohua Yi was with School of Civil and Environmental Engineering, Georgia Institute of Technology (current address: ExxonMobil Upstream Research Company at Houston, TX 77389; e-mail: yixhzju@gmail.com)

Yang Wang is with the School of Civil and Environmental Engineering, Georgia Institute of Technology, Atlanta, GA 30332 USA. (e-mail: yang.wang@ce.gatech.edu).

Terence Wu is with DIRECTV, El Segundo, CA 90245 USA (e-mail: wterence@gmail.com).

Manos M. Tentzeris is with School of Electrical and Computer Engineering, Georgia Institute of Technology, Atlanta, GA 30332 USA (e-mail: etentze@ece.gatech.edu).

enhances manufacturability, and effectively allows individual sensor identification. RFID could tremendously enhance the applicability and scalability for large-area wireless sensor networks. In this paper, a low-cost RFID-enabled passive strain sensor has been developed based on a folded patch antenna design. Laboratory experiments show that the resonance frequency of the proposed antenna changes even for a small amount of strain/deformation, thus featuring high strain sensing resolution. The read range of the fabricated proof-of-concept prototype reaches up to 2.5 meters, and a strain sensitivity of −760 Hz/με (equivalent to normalized strain sensitivity of -0.74 ppm/με) has been demonstrated. Furthermore, this paper presents a novel theoretical formulation for the strain sensitivity of the antenna sensor, considering for the first time the changes in the value of the substrate dielectric constant due to local strain. The dielectric constant change is experimentally measured using a specially designed resonator. Finally, the dielectric constant variation is incorporated in a mechanics-electromagnetics coupled model for more accurate simulation results.

The paper is organized as follows. Section II describes strain sensing mechanism of the folded patch antenna sensor, and the mechanics-electromagnetics coupled simulation model. Section III presents experimental strain sensing results of the antenna sensor. To understand the discrepancy in normalized strain sensitivity between simulation and experiments, Section IV proposes a strain sensitivity formulation that considers the substrate dielectric constant change under strain. Section V presents experimental validation results of the dielectric constant change. Finally, Section VI provides a summary and discussion.

II. SENSING MECHANISM AND MECHANICS-ELECTROMAGNETICS COUPLED SIMULATION

In this section, the strain sensing mechanism of an antenna sensor is first presented. Based on the sensing mechanism, a folded patch antenna sensor is designed through mechanics-electromagnetics coupled simulation.

Before introducing the strain sensing mechanism of the antenna sensor, the definition of mechanical strain ε is provided as follows. In engineering, strain is usually defined as relative change of length when an object deforms:

$$\varepsilon = \frac{L - L_0}{L_0} \qquad (1)$$

where L_0 is the original length of the object; L is the final deformed length. The unit of strain is dimensionless, which is usually denoted as με (microstrain). One με means 1×10^{-6} or 1 ppm (parts per million) relative change in length. Notation for strain, ε, can be easily confused with dielectric constant in antenna literature. To avoid confusion, β_r is used herein to represent relative dielectric constant.

To drastically reduce the size of the sensors that typically use a half-wavelength patch antenna, a quarter-wavelength folded patch antenna topology is adopted [16]. For a quarter-wave folded patch antenna, the resonance frequency of the antenna under strain, $f_{R\varepsilon}$, can be approximated with the following equation.

$$f_{R\varepsilon} = \frac{c}{4[L(1+\varepsilon) + L'(1-v\varepsilon)]\sqrt{\beta_r}} \qquad (2)$$

In the above equation, c is the speed of light in free space, L is the patch length, v is the Poisson's ratio, which is the absolute ratio between transverse strain and longitudinal strain of the antenna when force is applied longitudinally, β_r is the relative dielectric constant of the substrate, and L' is the compensating additional length due to edge-fringing field defined in the following equation [17]:

$$L' = 0.412H \frac{(\beta_{r,eff} + 0.3)(W/H + 0.264)}{(\beta_{r,eff} - 0.258)(W/H + 0.813)} \qquad (3)$$

where H is the antenna substrate thickness and $\beta_{r,eff}$ represents the effective dielectric constant of the microstrip patch, which approximately equals β_r [16]. Since the substrate thickness H is usually much smaller than the patch length, the resonance frequency is primarily determined by the patch length L. The relationship between the resonance frequency $f_{R\varepsilon}$ and the applied strain ε can be estimated in the following equation:

$$f_{R\varepsilon} \approx \frac{c}{4(L+L')\sqrt{\beta_r}(1+\varepsilon)} \approx f_{R0}(1-\varepsilon) \qquad (4)$$

The ε in Eq. (4) is expressed in με or 1ppm, which is a small number. Even when ε approach 10,000 με, it is still much smaller than 1, which means Eq. (4) still holds. In practice, due to sensor fabrication and installation tolerances, the "zero-strain" resonance frequencies of different individually fabricated antenna sensors can slightly differ. To alleviate the effect of this variability on strain measurements, the concept of normalized resonance frequency change is introduced. The resonance frequency change is normalized by the initial "zero-strain" resonance frequency (i.e. f_{R0} at zero strain level):

$$\Delta f_N = \frac{f_{R\varepsilon} - f_{R0}}{f_{R0}} \approx -\varepsilon \qquad (5)$$

where Δf_N represents the normalized frequency change. As shown in Eq. (5), the normalized strain sensitivity is close to −1, which means 1με strain increase on the sensor generates 1ppm decrease in resonance frequency.

Although the above formulations provide estimation to the antenna frequency change under strain, finite element simulations can provide a more accurate prediction, particularly when the antenna shape has irregular mechanical features such as vias going through the substrate. To efficiently model and
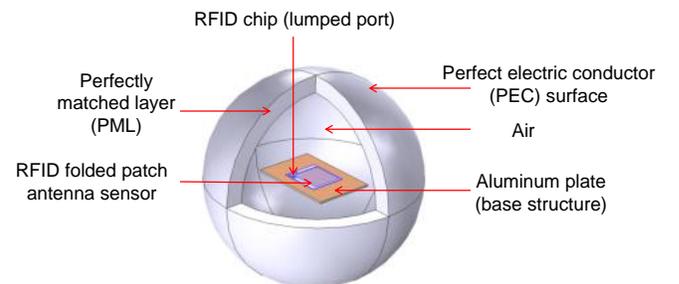
Fig. 1. Multi-physics simulation model of the folded patch antenna sensor using COMSOL

simulate both the mechanical and electromagnetic phenomena involved in the antenna sensor, multi-physics simulation software tools are preferred. To this end, Fig. 1 shows the simulation model for an RFID folded patch antenna sensor in COMSOL, the commercial software tools are capable of multi-physics simulations [18]. The antenna sensor is bonded at the center of an aluminum plate. The RFID chip is simulated as a lumped port with the electrical impedance ($Z_c = 13.3-122\,j\,\Omega$) of the chip. The bonding between the bottom copper cladding (i.e. effectively the ground plane) of the antenna sensor and the aluminum plate is assumed to be ideal. For the implementation of this in the simulated model, the mechanical elements of these two components share the same nodes at the interface. Similarly, the bonding between the top/bottom copper cladding and the antenna substrate is assumed to be ideal. The mechanical module in COMSOL is first used to accurately simulate the deformed antenna shape. When a tensile load is applied to the aluminum plate (base structure), the strain propagates through the antenna substrate to the top copper cladding.

Using the newly deformed shape, the antenna resonance frequency under strain is then accurately quantified through the electromagnetics module in COMSOL for the same finite element model. For the electromagnetic simulation, the antenna sensor, together with the mounting aluminum plate, is placed at the center of an air sphere. At the outer surface of the air sphere, the absorbing boundary condition is set as a perfectly matched layer (PML) [19]. The PML boundary condition allows the

(a) Simulated S_{11} plots at different strain levels

(b) Normalized resonance frequency change Δf_N versus strain ε ($f_{R0} = 911.6$ MHz)

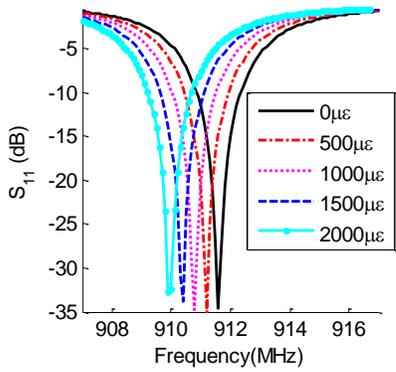Fig. 2 Simulation results for the folded patch antenna

electromagnetic wave emitted by the antenna sensor to pass through with minimal spurious numerical reflections, which mimics the propagation of electromagnetic wave into infinite free space. The PML enclosed by a PEC (perfect electric conductor) surface truncates the simulation domain to be finite. The two copper cladding layers, i.e. top and bottom, are meshed using shell elements with a thickness of 0.017mm. The copper and aluminum materials are modeled as perfect electric conductor (PEC) in electromagnetic simulation.

For the mechanical simulation, tetrahedral and prism elements are adopted to model solid structures such as the aluminum specimen and substrate. To model the shell structures, such as top and bottom copper cladding, triangular elements are used to reduce discretization error and quadrilateral elements are adopted to achieve better numerical accuracy. For the electromagnetic simulations, the air sphere and the PML layer are similarly modeled as tetrahedral and prism elements.

In the mechanical simulations, only the aluminum plate and the antenna sensor (including the substrate and two copper layers) are involved, while the air sphere is neglected. Prescribed displacements are applied at the two ends of the aluminum plate, so that five different strain levels (from 0 to 2,000με at an increment step of 500με) are generated in the aluminum plate. After the mechanical simulation at each strain level, the deformed meshing is directly used for electromagnetic simulation to determine the resonance frequency of the antenna sensor under strain. During the electromagnetic simulation, a frequency domain solver is used to calculate the return loss (reflection coefficient) S_{11}. S_{11} quantifies the impedance matching, and effectively the power transfer quality, between the lumped port (RFID chip) and the antenna. A smaller S_{11} value means the RFID chip can emit more electromagnetic energy through the antenna into the air, indicating better matching and higher antenna efficiency. The simulated frequency range is 907.5 ~ 916.5 MHz with a frequency step of 0.05 MHz. The average computation time for one frequency point is about 503 seconds. The total computation time is roughly proportional to the number of strain steps to be simulated, and the number of frequency points per strain step. In this study with five strain steps and 181 frequency points per strain step, the total computing time on an 8GB Intel Core 2 Duo CPU machine is 126 hours and 27 minutes.

Fig. 2(a) shows a simulated S_{11} plot of the folded patch antenna sensor at five different strain levels. At each strain level, the antenna resonance frequency can be extracted by peak picking. A clear and distinct decrease in the antenna resonance frequency is observed when strain increases. As previously mentioned, at zero strain level, the antenna resonance frequency is found to be 911.6 MHz. At 2,000 με, the resonance frequency decreases to 909.95 MHz.

The resonance frequency at each strain level is extracted from Fig. 2(a). The corresponding normalized resonance frequency change is then calculated according to Eq.(5). Fig. 2(b) plots the relationship between the normalized resonance frequency change and strain. The coefficient of determination
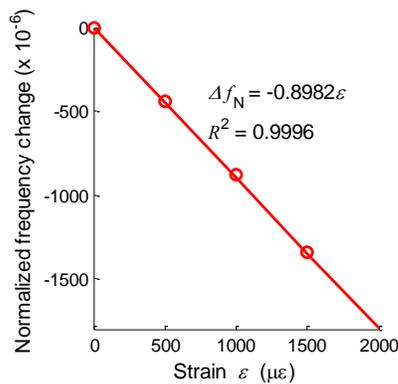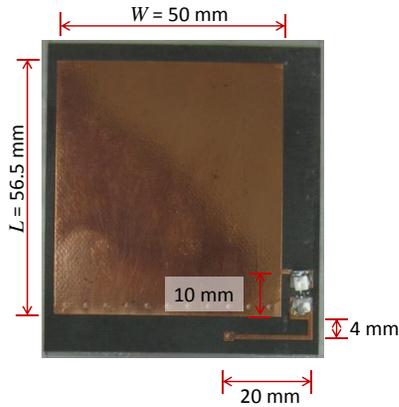
Fig. 3 Photo of the quarter wave patch antenna sensor. The substrate thickness *H* is 0.787 mm

Fig. 4 The measurement setup of the RFID antenna sensor

(R^2) is 0.9996, which indicates a good linearity between the normalized frequency change and the simulated applied strain. The normalized strain sensitivity is −0.8982 ppm/μɛ, which means 1 μɛ strain increase experienced by the folded patch antenna causes 0.8982 ppm decrease in resonance frequency. The magnitude of the normalized strain sensitivity is lower than 1 ppm/μɛ. Since shear lag effect exists in relatively thick substrates, the strain experienced by the top copper antenna pattern is lower than the strain experienced by the base structure, which partly reduces the normalized strain sensitivity. The simulation results will be further compared with experimental results to validate whether the shear lag effect is the only reason causing a smaller normalized strain sensitivity.

After optimization through simulation, the antenna sensor design is finalized and ready for fabrication. Fig. 3 shows the photo of a fabricated folded patch antenna. The smaller sensor footprint achieved by the folded patch antenna topology is more suitable for measuring strain/stress distribution as well as allowing for easier mounting. It should be noted that the size reduction also comes at the cost of additional via connections and a reduced radiation directivity [16]. For maximum power transfer from the antenna to the RFID chip, the conjugate matching technique is required to maximize the transmission coefficient. In this design, the conjugate matching is achieved by the utilization of a matching inductance generated by the 24mm short circuit stub connected to the other pin (ground line) of the chip. Without loss of generality and for proof-of-concept purposes, the benchmarking antenna sensor prototype is built by standard PCB fabrication on a Rogers 5880 substrate, a glass microfiber reinforced poly-tetra-fluoro-ethylene (PTFE) composite with dielectric constant of 2.2 under zero-strain. The substrate thickness is *H*=0.787 mm and the copper cladding thickness is 17 μm. The planar dimensions of the copper antenna are *L*×*W* = 56×50 mm.

III. SENSOR SETUP AND MEASUREMENT

The measurement setup for wireless strain sensing is shown in Fig. 4 . The system consists of an RFID reader for wireless
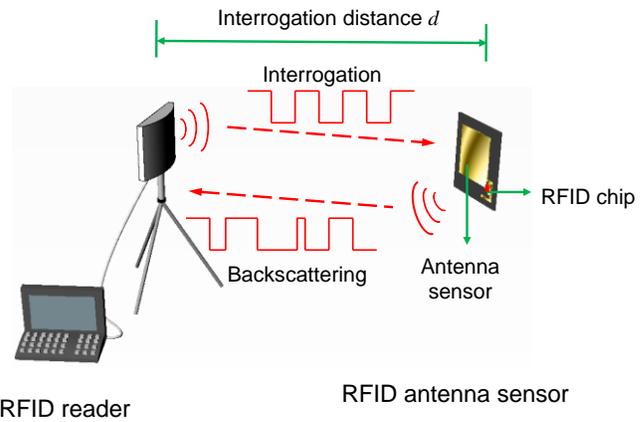
interrogation, as well as an RFID antenna sensor attached to an aluminum specimen under strain (introduced by a tensile testing machine). When a reader emits an interrogation electromagnetic wave to the completely-passive antenna sensor, both the antenna sensor and the surrounding environment reflect back to the reader antenna. The large reflection from the environment can overwhelm the sensor response. To differentiate the sensor response from environmental reflections, the time gating technique [12] or the open-and-short circuit response is needed to control the sensor reflection [13]. In this study, an RFID chip is used to efficiently generate a modulated backscattered signal to differentiate the sensor response from the non-modulated environmental/background reflections [20]. Furthermore, the RFID chip is priced less than ten cents, making this approach particularly attractive for mass production. The SL3ICS1002 chip (manufactured by NXP Semiconductors) is chosen as the RFID chip; the small footprint of the chip causes minimal disturbance to the mechanical strain transfer from the aluminum specimen to the patch antenna.

The patch antenna operates in a "dual-mode," as both the communication component and the strain sensing element. A Tagformance RFID reader (made by Voyantic Ltd.) is used to measure the interrogation power threshold of the sensor, which is the minimum interrogation power from reader that is just
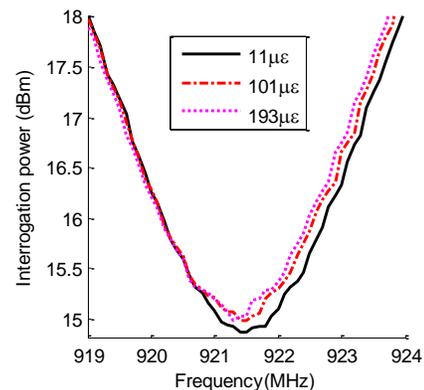

Fig. 5 Interrogation power of the reader required to activate the RFID chip at three different strain levels.
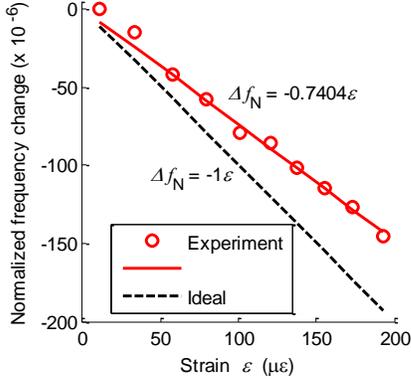
Fig. 6 Normalized strain sensitivity of the folded patch antenna sensor from experimental measurements

enough to activate the RFID chip. To guarantee reading at different angles between the sensor and the reader antenna, a circular polarized antenna (S8658WPC made by Cushcraft Corporation) is used at the reader side to interrogate the linearly polarized antenna sensor. Within the specified frequency range, the interrogation process measures the interrogation power threshold required of the reader for activating the sensor. The resonance frequency of the antenna sensor is identified as the interrogation frequency at which the least amount of interrogation power is required to activate the sensor. Because there is no on-board strain signal digitization by the sensor, the sensing resolution and accuracy is highly dependent on the reader that acts similar to a wireless ADC (analog-to-digital converter). The Tagformance reader is capable of adjusting the interrogation power with 0.1dBm accuracy, while sweeping through the frequency range at 0.1 MHz resolution. To further improve the measurement precision and reduce the ambient noise effect, five power threshold samples at each strain level of the same prototype are averaged to ensure reliable sensor readings and maintain relatively reasonable measurement time. The averaged curve is then applied with 4th-order curve fitting. The interrogation power threshold for different strain levels is shown in Fig. 5, when the sensor is interrogated from a distance of 30 cm, which is chosen for proof-of-concept test. More details about the experimental setup can be found in [21, 22].

Since the interrogation power level is relatively flat around the resonance frequency, the threshold data within 3dB bandwidth is used to determine the resonance frequency. Fig. 6 plots the normalized resonance frequency change, calculated according to Eq. (5), against the strain level. The normalized strain sensitivity is -0.7404 ppm/με, which is obtained as the slope of the linear regression. More extensive experiments have been conducted to verify the sensor performance under different loading conditions and the results show relatively consistent strain sensitivities [20, 21]. The difference between the experimental and the simulated data in Fig. 6 is caused by the substrate expansion and the changes in the material's dielectric properties under strain, which is not accounted for in the simulation model. A thorough analysis of the substrate effect is addressed in Section IV.

IV. THEORETICAL DERIVATION OF STRAIN SENSITIVITY

Comparing Fig. 2 and Fig. 6, there is an obvious discrepancy between the measured and simulated normalized strain sensitivities. The main reason causing the discrepancy can be due to the relative dielectric constant variation over strain. Contrary to ideal materials, small voids always exist in practical substrate materials. The distortion of the voids under strain affects the dielectric constant of the substrate, although very limited information is available from the manufacturer datasheet for the substrate. The other reason could be the strain transfer ratio between the top copper cladding of the sensor and aluminum plate. During the measurements, the sensor is bonded to the structural surface by superglue. The strain experienced by the top copper cladding is smaller than the strain on the bottom copper ground plane and the structural surface, due to shear lag effect through the 0.787 mm Rogers material. To achieve a more accurate prediction, the relative dielectric constant-strain relationship and the correct strain transfer ratio need to be implemented in the COMSOL simulations. To describe this phenomenon, a new strain sensitivity model is proposed in this section for the first time.

The proposed model addresses two factors affecting the measured sensitivity: i) the efficiency of mechanical strain transfer from the base structure to the top surface of the RFID antenna sensor, denoted as η_m ; ii) the substrate dielectric constant change due to strain, denoted as $\Delta\beta_r$. The strain transfer ratio, η_m, is defined as:

$$\eta_m = \frac{\varepsilon_t}{\varepsilon} \tag{6}$$

where ε_t is the tensile strain experienced on the top copper cladding, and ε is the actual strain on the base structural surface. With a firm bonding between the base structure and the bottom copper cladding of the antenna sensor, ε is also the tensile strain at the bottom copper cladding. In order to quantify the strain transfer ratio η_m, mechanical strain transfer experiments can be conducted to determine the ratio at different strain levels.

In order to determine the dielectric constant change $\Delta\beta_r$, a simple half-wave resonator is designed (Fig. 7). The dimensions of the resonator are tuned to maintain its resonance frequency around 950 MHz. Considering the dielectric constant variation over strain, when the strain is applied to the bonded structural surface, the resonance frequency at strain ε_t can be estimated as:

Fig. 7. Resonator design for characterizing dielectric constant change against strain.

$$f_{R\varepsilon_t} \approx \frac{c}{2(L+\Delta L)\sqrt{(\beta_{r0}+\Delta\beta_r)}} \tag{7}$$

where ΔL is the change of center transmission line length due to strain ε_t; $\Delta\beta_r$ is the dielectric constant change with strain ε_t. The resonance frequency change between zero strain and ε can be derived as:
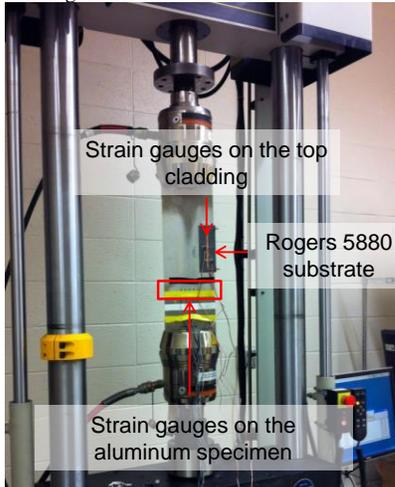
$$
\begin{aligned}
\Delta f &= f_{R\varepsilon_t} - f_{R0} \\
&= \frac{c}{2}\left(\frac{1}{(L+\Delta L)\sqrt{(\beta_{r0}+\Delta\beta_r)}} - \frac{1}{L\sqrt{\beta_{r0}}} \right) \\
&= \frac{c\left(1-\sqrt{(1+\Delta\beta_r/\beta_{r0})}\right)}{2(L+\Delta L)\sqrt{(\beta_{r0}+\Delta\beta_r)}} - f_{R0}\frac{\Delta L}{(L+\Delta L)}
\end{aligned}
\tag{8}
$$

According to Taylor expansion:

$$\sqrt{1+\frac{\Delta\beta_r}{\beta_{r0}}} \approx 1 + \frac{1}{2}\frac{\Delta\beta_r}{\beta_{r0}} - \frac{1}{8}\left(\frac{\Delta\beta_r}{\beta_{r0}}\right)^2 + \cdots \tag{9}$$

Strain gauges on the top cladding

Rogers 5880 substrate

Strain gauges on the aluminum specimen

(a) Specimen configuration

Strain gauges on the top cladding

Rogers 5880 substrate

Strain gauges on the aluminum specimen

(b) Experimental setup

Fig. 8 Experimental setup for strain transfer calibration

Since $\Delta\beta_r \ll \beta_{r0}$, higher order terms of $\Delta\beta_r/\beta_{r0}$ in Eq. (9) are neglected, Eq. (8) is further simplified as:

$$
\begin{aligned}
\Delta f &\approx -\frac{c\Delta\beta_r}{4\beta_{r0}(L+\Delta L)\sqrt{(\beta_{r0}+\Delta\beta_r)}} - f_{R0}\varepsilon_t \\
&= -f_{R\varepsilon_t}\frac{\Delta\beta_r}{2\beta_{r0}} - f_{R0}\varepsilon_t
\end{aligned}
\tag{10}
$$

The resonance frequency change due to dielectric constant change and applied strain can be de-coupled according to Eq. (10). The relative dielectric constant change, when base structure is under strain ε, is thus derived:

$$\Delta\beta_r = -\frac{2\beta_{r0}}{f_{R\varepsilon_t}}\left(\Delta f + f_{R0}\eta_m\varepsilon\right) \tag{11}$$

Using Eq. (11), the dielectric constant $\Delta\beta_r$ at different strain levels ε can be calculated from tensile testing results of the resonator, and then implemented in COMSOL for the accurate simulation of antenna behavior under strain. Upon fabrication of the resonator, tensile testing is performed and the results are presented in the following section.

V. EXPERIMENTAL DETERMINATION OF DIELECTRIC CONSTANT CHANGE OVER STRAIN

This section presents the experimental results of the resonator introduced in Section IV. A tensile test of the resonator is first conducted for the characterizing of the strain transfer ratios, and the results are presented in Section A. Another tensile test of the resonator is then performed to characterize the dielectric constant change under strain, and the results are presented in Section B.

A. Strain transfer test

The strain transfer ratio η_m is calibrated using a fabricated resonator bonded on an aluminum specimen. Fig. 8 shows the experimental setup of the strain transfer calibration test. Five metal foil strain gauges are installed in the center area of the aluminum specimen. To check the strain transfer ratio, another three metal foil strain gauges are installed on the top copper cladding of the resonator. A National Instruments strain gauge module (NI 9235), together with a CompactDAQ Chassis (NI cDAQ-9172), is used for collecting data from metal foil strain gauges. The axial force applied by the tensile testing machine is configured so that approximately a 500 με strain increment is achieved at each loading step till the maximum strain around 2,000 με.

Fig. 9 summarizes the experimental results of the strain transfer test. Fig. 9(a) shows the differences between strain on the aluminum specimen and strain on the top copper cladding of the substrate material. As the applied strain increases, the strain difference also increases gradually. Fig. 9(b) shows the strain transfer ratio between the two layers. The strain transfer ratio, η_m, is around 90% when the applied strain is within the range of 2,000 με. According to Eq. (11), the strain transfer
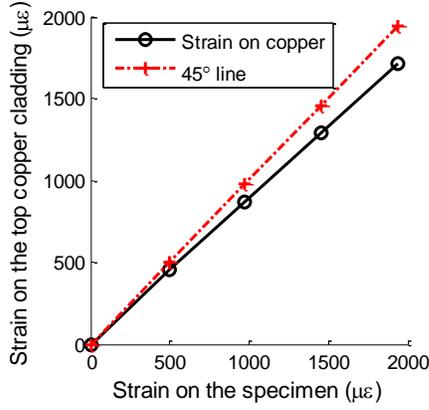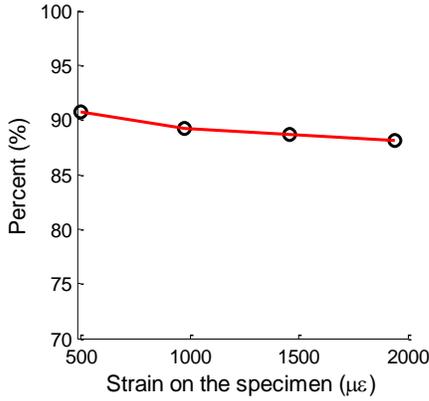
(a) Strain differences

(b) Strain transfer ratio η_m

Fig. 9 Experimental results for strain transfer ratio

ratio will later be used to calibrate the experimentally verified dielectric constant change due to strain.

B. Resonance frequency test

To calculate $\Delta\beta_r$ according to Eq. (11), the resonator is further tested to evaluate its resonance frequency change under strain. Fig. 10 shows the experimental setup for the tensile test. The resonator is installed along the side of an aluminum specimen, together with five metal foil strain gauges in the center area of the specimen. The S_{21} coefficient of the resonator
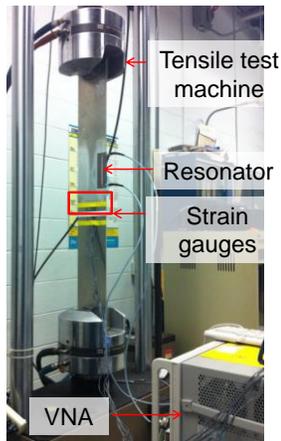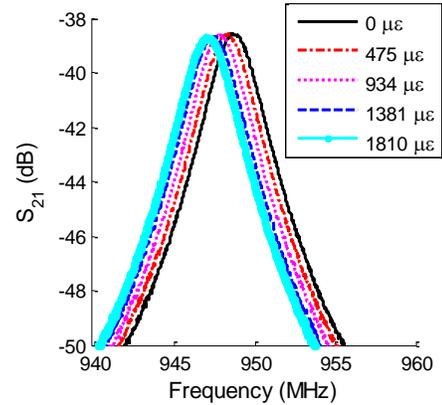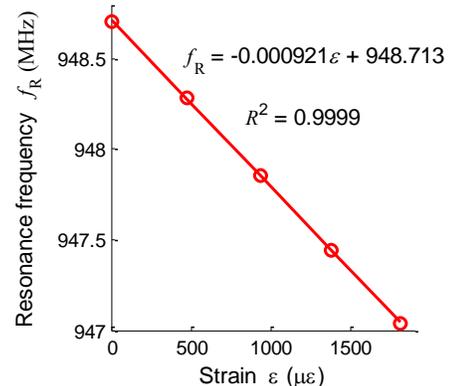

Fig. 10 Experimental setup for dielectric constant characterization

is measured by a vector network analyzer (VNA). Again, the tensile testing machine is configured so that approximately a 500 µε strain increment is achieved at each loading step. The test starts with zero strain, and ends at around 2,000 µε. Fig. 11 (a) plots the measured S_{21} of the resonator at five different strain levels. The strain levels in Fig. 11 (a) are the average values among the five metal foil strain gauges, after strain transfer calibration [21]. The S_{21} value reaches its maximum at the resonance frequency of the resonator. For example, at zero strain, the resonance frequency is f_{R0} = 948.705 MHz. Fig. 11 (a) shows a clear resonance frequency decrease during strain increase. For accuracy, a 4th order polynomial curve fitting is performed to the peak area of each plot [21]. The fitted 4th order polynomial is used for the identification of the resonance frequency that corresponds to the maximum S_{21}. Fig. 11 (b) shows the relationship between the resonance frequency and the applied strain. When the strain ε_t is at 1,810 µε, the resonance frequency changes to 947.04 MHz. According to Eq. (11), the corresponding dielectric constant change, $\Delta\beta_r$, at different strain levels can be calculated and the results are shown in Fig. 12. As shown in this figure, the dielectric constant of the substrate decreases gradually as the applied strain increases. The polymer chain of substrate material PTFE is re-oriented in the direction of applied strain, which reduces motion of polymer group and material polarization [23, 24].

(a) Measured S_{21} plots at different strain levels

(b) Resonance frequency change under strain

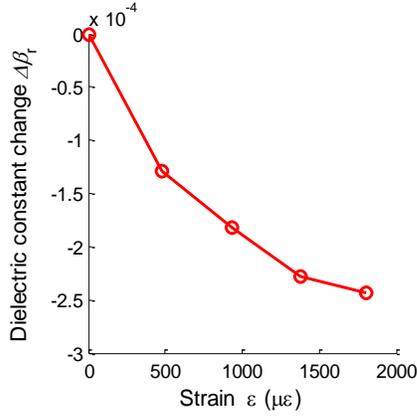Fig. 11 Experimental results for dielectric constant change

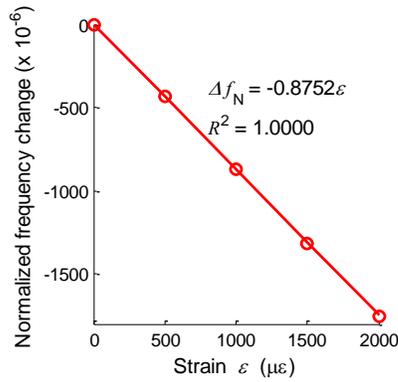Fig. 12. Dielectric constant change under strain

Fig. 13. Simulation results for the folded patch antenna after implementing dielectric constant changes

Overall, the dielectric constant decreases from 2.2 to 2.1998, when strain increases from 0 to 1,810 µε. Li [23] studied the mechanical strain effect on PTFE material in a large deformation range. When the mechanical strain is less than 25%, similar amount of dielectric constant change is observed in a frequency band of 100 kHz. The relationship between the dielectric constant change and applied strain is not linear, which confirms the necessity of dielectric constant calibration under strain for higher simulation accuracy. Calculated from Eq. (11), the relationship between the dielectric constant variation and the applied strain is to be imported into the mechanics-electromagnetics coupled COMSOL simulation.

Considering the dielectric constant change under strain, the updated multi-physics COMSOL simulation results are shown in Fig. 13. The corresponding normalized strain sensitivity is -0.8752 ppm/µε, which is about 0.023 ppm/µε smaller than the simulation results without considering dielectric constant change under strain effect. The smaller normalized strain sensitivity is closer to the experimental results that the inclusion of dielectric constant change effect does improve the coupled simulation accuracy. Nevertheless, the simulated strain sensitivity is still larger than the experimental results and deserves further investigation. One possible explanation may be relevant to the structure of the resonator presented in Section IV. The resonator includes not only the center transmission line, but also two feeding lines for the measurement at the two ports. Under mechanical loading, the two feeding lines also

deform and thus contribute to the overall resonance frequency change (in addition to the contribution from the dielectric constant change). This effect from the feeding lines is difficult to quantify, and may reduce the accuracy of the dielectric constant characterization.

VI. CONCLUSION

A low-cost passive RFID sensor, which is based on a folded patch antenna in UHF frequency range, has been developed for measuring strain on metallic surfaces. The resonance frequency of the antenna varies as the antenna elongates under strain. Detailed theoretical formulations and experiments demonstrate that the change in dielectric constant due to strain affects the resonance frequency shift, and needs to be considered in high-fidelity multi-physics simulation of the antenna sensor. To address this fundamental issue in antenna sensors for strain sensing, a new strain sensitivity model is proposed for considering the substrate dielectric constant change under strain. The tensile testing of a resonator is devised and performed for quantifying both strain transfer ratio and dielectric constant change. Besides antenna sensors for strain sensing, the discovered results can also be used in the analysis of flexible optical and high frequency electronics.

REFERENCES

[1] H. Sohn, C. R. Farrar, F. M. Hemez, D. D. Shunk, D. W. Stinemates, B. R. Nadler, and J.J. Czarnecki, "A Review of Structural Health Monitoring Literature: 1996-2001," Los Alamos National Laboratory, Los Alamos, NM Report No. LA-13976-MS, 2003.

[2] W. C. Michie, B. Culshaw, S. S. J. Roberts, and R. Davidson, "Fiber optic technique for simultaneous measurement of strain and temperature variations in composite materials," in *Proceedings of SPIE, Fiber Optic Smart Structures and Skins IV*, vol. 1588, Boston, MA, 1991.

[3] W. M. Murray and W. R. Miller, *The Bonded Electrical Resistance Strain Gage: An Introduction*. New York, NY: Oxford University Press, 1992.

[4] L. Liu and F. Yuan, "Wireless sensors with dual-controller architecture for active diagnosis in structural health monitoring," *Smart Materials and Structures,* vol. 17, p. 025016, 2008.

[5] N. Kurata, B. F. Spencer, and M. Ruiz-Sandoval, "Risk monitoring of buildings with wireless sensor networks," *Structural Control Health Monitoring,* vol. 12, pp. 315-327, June 6, 2005 2005.

[6] P. Glynne-Jones and N. M. White, "Self-powered systems: a review of energy sources," *Sensor Review,* vol. 21, pp. 91-98, 2001.

[7] L. Wang and F. G. Yuan, "Energy harvesting by magnetostrictive material (MsM) for powering wireless sensors in SHM," in *Proceedings of SPIE, Sensors and Smart Structures Technologies for Civil, Mechanical, and Aerospace Systems*, vol. 6529, San Diego, CA, 2007.

[8] S. P. Beeby, M. J. Tudor, and N. M. White, "Energy harvesting vibration sources for microsystems applications," *Measurement Science and Technology,* vol. 17, pp. R175-R195, 2006.

[9] F. Gasco, F. Paolo, J. Braun, J. Smith, P. Stickler, and L. DeOto, "Wireless strain measurement for structural testing and health monitoring of carbon fiber composite," *Journal of Composites: Part A,* vol. 42, pp. 1263-1274, 2011.

[10] Y. Jia, K. Sun, F. J. Agosto, and M. T. Quinones, "Design and characterization of a passive wireless strain sensor," *Measurement Science and Technology,* vol. 17, pp. 2869-2876, Nov 2006.

[11] K. J. Loh, L. J. P., and N. A. Kotov, "Passive wireless strain and pH sensing using carbon nanotube-gold nanocomposite thin films," in *Proceedings of SPIE, Sensors and Smart Structures Technologies for Civil, Mechanical, and Aerospace Systems*, vol. 6529, San Diego, CA, 2007.

[12] D. J. Thomson, D. Card, and G. E. Bridges, "RF cavity passive wireless sensors with time-domain gating-based interrgoation for SHM of civil structures," *IEEE Sensors Journal,* vol. 9, pp. 1430-1438, 2009.

[13] S. Deshmukh and H. Huang, "Wireless interrogation of passive antenna sensors," *Measurement Science and Technology,* vol. 21, 2010.

[14] H. Huang, "Flexible wireless antenna sensor: a review," *IEEE Sensors Journal,* vol. 13, pp. 3865-3872, 2013.

[15] M. Keskilammi, L. Sydanheimo, and M. Kivikoski, "Radio frequency technology for automated manufacturing and logistics control. Part 1: passive RFID systems and the effects of antenna parameters on operational distance," *The International Journal of Advanced Manufacturing Technology,* vol. 21, pp. 769-774, 2003.

[16] R. Garg, P. Bhartia, I. Bahl, and A. Ittipiboon, *Microstrip Antenna Design Handbook*. Norwood, MA: Artech House, 2001.

[17] K. Finkenzeller, *RFID Handbook*, 2nd ed. New York: John Wiley & Sons, 2003.

[18] COMSOL, "The COMSOL multiphysics reference guide," COMSOL, Inc., Burlington, MA, USA, 2012.

[19] J. M. Jin, *The Finite Element Method in Electromagnetics*, 2nd ed. New York: John Wiley & Sons, Inc., 2002.

[20] A. Rida, L. Yang, and M. M. Tentzeris, *RFID-enabled Sensor Design and Applications*. Norwood, MA: Artech House, 2010.

[21] X. Yi, T. Wu, Y. Wang, R. T. Leon, M. M. Tentzeris, and G. Lantz, "Passive wireless smart-skin sensor using RFID-based folded patch antennas," *International Journal of Smart and Nano Materials,* vol. 2, pp. 22-38, Jan 2011.

[22] X. Yi, C. Cho, J. Cooper, Y. Wang, M. M. Tentzeris, and R. T. Leon, "Passive wireless antenna sensor for strain and crack sensing-electromagnetic modeling, simulation, and testing " *Smart Materials and Structures,* vol. 22, p. 085009, 2013.

[23] L. Li, "Dielectric Properties of Aged Polymers and Nanocomposites," Ph.D., Materials Science and Engineering, Iowa State University, Ames, Iowa, 2011.

[24] S. O. Kasap, *Principles of Electrical Engineering Materials and Devices*, 3rd ed. New York, NY: McGraw-Hill, 2006.